

Basic Oxygen Steelmaking Slag: Formation, Reaction, and Energy and Material Recovery

Li, Z., Li, J., Spooner, S. & Seetharaman, S.

Published PDF deposited in Coventry University's Repository

Original citation:

Li, Z, Li, J, Spooner, S & Seetharaman, S 2022, 'Basic Oxygen Steelmaking Slag: Formation, Reaction, and Energy and Material Recovery', *Steel Research International*, vol. 93, no. 3, 2100167

<https://dx.doi.org/10.1002/srin.202100167>

DOI 10.1002/srin.202100167

ISSN 1611-3683

ESSN 1869-344X

Publisher: Wiley

This is an open access article under the terms of the Creative Commons Attribution License, which permits use, distribution and reproduction in any medium, provided the original work is properly cited.

Basic Oxygen Steelmaking Slag: Formation, Reaction, and Energy and Material Recovery

Zushu Li,* Juncheng Li, Stephen Spooner, and Sridhar Seetharaman

Basic oxygen steelmaking (BOS) slag, a product of hot metal element (e.g., Si, Mn, Fe, P) oxidation and flux (e.g. lime, dolomite) dissolution, plays a critical role in the production of high-quality crude steel, although its behavior inside the BOS vessel (formation and reaction with metal droplets and gas) is still not clear and its recycling has always been challenging. Herein, examples of BOS-slag-related research conducted by the present authors are introduced, in addition to a critical review of relevant research reported in the literature. This includes four important topics: 1) slag formation, i.e., dissolution of lime in the BOS slag; 2) in situ observation of high-temperature behavior of BOS slags; 3) transient phenomena in BOS slags due to metal droplet–slag–gas reactions; and 4) energy and material recovery from molten BOS slags. This article aims to provide state-of-the-art understanding and new research ideas on these research topics. An emphasis is placed on methods that seek to in situ probe the evolution of the slag and to document its physical and chemical changes.

and flux (e.g., lime, dolomite) dissolution, plays a critical role in the production of high-quality crude steel.

All elements present in the hot metal charged in the BOS converter are thermodynamically very unstable with respect to their oxides when exposed to the oxygen jet at the BOS operating temperatures. Thus, carbon, silicon, manganese, phosphorus, and the iron itself all tend to oxidize very rapidly to form CO (or CO₂), SiO₂, MnO, P₂O₅, and FeO (or Fe₂O₃), respectively. In the BOS practice, large quantities of iron and silicon are initially oxidized to give a liquid, predominantly binary, FeO–SiO₂ slag, which floats on top of the metal pool. Usually lime (CaO) is rapidly added to “neutralize” this acid FeO–SiO₂ slag and produce a “basic” multicomponent FeO–SiO₂–CaO–MnO–Al₂O₃–MgO–P₂O₅ slag. This basic

1. Introduction

The basic oxygen steelmaking (BOS) process produced over 70% of the global crude steel in 2018,^[1] generating 100 to 150 kg of slag (“BOS slag”) for every tonne of crude steel produced. BOS slag, a product of hot metal element (e.g., Si, Mn, Fe, P) oxidation

slag produces the correct partition of metalloids, particularly phosphorus, between the slag and metal and also protects the basic vessel lining (usually magnesite, MgO). Over the entire blowing period of the BOS process, this basic slag is emulsified with a large amount of gas bubbles and metal droplets, and the gas–slag–metal droplet reactions control the element transfer between the steel and slag (e.g., phosphorus removal and reversion) and subsequently the productivity and crude steel quality, which greatly attracts great interest from academics to understand the transient phenomena in the gas–BOS slag–metal droplet system. After completing its refining function in the BOS process, the hot BOS slag is poured into a slag pot. The BOS slag was considered a waste in old times but now as a secondary resource because it contains a large amount of thermal energy (temperature up to 1700 °C), chemical energy (metallic and low-valence metallic oxides), and valuable materials (e.g., iron oxides).

The behavior of BOS slag inside the BOS vessel, e.g., formation and reaction with gas and metal droplets, is still not clear and its recycling, including energy and material recovery, has always been challenging. This article introduces some BOS-slag-related research conducted by the present authors, in addition to a critical review of relevant research reported in the literature. It covers the topics of lime dissolution (slag formation), high-temperature-behavior interrogation through in situ observation, slag–metal droplet reaction mechanisms (spontaneous emulsification), and recovery of energy and materials from the molten BOS slag. This article aims to provide state-of-the-art understanding on relevant research topics and point out new research directions.

Z. Li
WMG
University of Warwick
Coventry CV4 7AL, UK
E-mail: z.li.19@warwick.ac.uk

J. Li
Department of Materials Science and Engineering
Jiangsu University
Jiangsu 212013, P. R. China

S. Spooner
College of Engineering
Swansea University
Swansea SA1 8EN, UK

S. Seetharaman
School for Engineering of Matter, Transport and Energy
Arizona State University
Tempe, AZ 85287, USA

 The ORCID identification number(s) for the author(s) of this article can be found under <https://doi.org/10.1002/srin.202100167>.

© 2021 The Authors. Steel Research International published by Wiley-VCH GmbH. This is an open access article under the terms of the Creative Commons Attribution License, which permits use, distribution and reproduction in any medium, provided the original work is properly cited.

DOI: 10.1002/srin.202100167

2. Lime Dissolution in BOS Slags under Varying Dynamic Conditions

BOS slag is formed by a chemical process involving the oxidation of elements (e.g., Si, Mn, Fe, P) from the metal bath and the dissolution of added solids such as lime, limestone, dolomite, other fluxes, and iron ore in the slag. Quick formation of a suitable slag in the BOS process, depending on the dissolution of lime in the slag, could increase the process productivity and improve the steel quality at reduced costs. The addition of CaO, “lime”, aids in slag formation by creating a lower-melting-temperature oxide mixture with the Fe, Si, and Mn oxides. The resulting slag (either a liquid or a solid–liquid mixture) has physical and chemical properties largely defined by the CaO/SiO₂ ratio, which govern the performance of the slag, with respect to e.g., phosphorous refining and material recovery. Lump lime is added to top-blown converters and top–bottom combined blown converters via conveyors after the start of oxygen blowing (i.e., “charging at ignition”) either in one go or by split additions over a period of time. For the bottom-blown converters, pulverized lime is injected through tuyeres. The importance of lime dissolution in the formation of BOS slag and the resultant metallurgical performance have driven extensive studies since the adoption of the BOS process. The purposes of the studies are to understand the lime dissolution mechanisms, promote lime dissolution in BOS slag, and increase the productivity and crude steel quality from the BOS process.

2.1. Experimental Research on Lime Dissolution in BOS Slag

The experimental techniques used to study lime dissolution in BOS slag and the influencing factors can be divided into five types: 1) under static conditions, 2) using a rotating rod/disc, 3) under increased/forced convection, 4) sampling from industry converters, and 5) via direct observation. All these methods have combined with ex situ characterization tools for postmortem examination, such as microstructure determination and composition analysis. The experimental techniques and research

outcomes are briefly summarized in Table 1 and explained subsequently.

Lime dissolution in BOS slag has been studied by various researchers under static conditions, i.e., no convection in the limeslag system, and the experimental setups and conditions can be found from the original reports.^[2–5] The lime–slag assemblies studied include mechanically mixing slag with lime particles,^[2] placing a piece of lime in slag,^[3] dipping a pressed and sintered lime rod (or cylinder) into stagnant slag,^[2,4,5] and packing the slag into a dense lime crucible.^[3]

To increase the dynamics of the lime dissolution during experiments, a rotating disk/cylinder technique was used to study the dissolution rate of dense lime specimens in calcium–aluminosilicate-based melts at the temperatures of interest.^[6–8] The measured dissolution rates were strongly dependent on the rotation speed of the lime sample, which indicates mass transfer in the slag phase to be a rate-limiting step. However, Deng et al.^[9] conducted computational fluid dynamics (CFD) calculation along with cold model experiments to investigate the effect of the rotating rod on the mass transfer. They concluded that a perfectly concentrically placed rotating rod such as in the experiments with the rotating disk/rod in molten slag^[6–8] creates no forced convection in the radial direction, which explains why mass transfer in the slag phase was found to be a rate-determining step.^[6–8] The forced convection in the radial direction is still limited even if the rotating rod is placed noncentrically in the slag phase.

It is perceived that forced convection is much more dominant than natural convection and diffusion in the BOS process. As discussed earlier, the rotating rod technique cannot enhance the mass transfer by forced convection. Various new experimental techniques have been proposed to introduce efficient mass transfer by forced convection. Deng et al.^[9,10] proposed a different laboratory technique to increase the convection in the molten slag containing a lime cube. That is, the molten slag with a lime cube inside was eccentrically stirred by a bar moving circularly between the center and wall of the crucible. It is evident that in this experiment a stirring rate of ≈100 rpm was found to be efficient to remove the interface layer(s) between the liquid

Table 1. Summary of experimental methods and findings for lime dissolution in BOS slag.

Experimental condition	Description and references	Brief summary of findings
Static conditions	Physically mixing slag with lime particles; ^[2] placing a lime piece in slag; ^[3] dipping a lime rod/disc into stagnant slag; ^[4] packing slag in a dense lime crucible ^[5]	(Ca, Fe)O solid solution next to lime particle and 2CaO–SiO ₂ (or 3CaO–SiO ₂) boundary layer next to slag at the lime particle–slag interface are kinetic barriers for lime dissolution
Rotating rod/disc	Rotating a lime disc/cylinder in molten slag ^[6–8]	Mass transfer in the slag phase is the limiting step of lime dissolution
Forced convection	Eccentrically stirring the molten slag (containing a lime cube); ^[9,10] stirring slag using a Mo impeller ^[11] or alumina impeller; ^[12] argon gas bubbling in slag via an iron tube ^[13,14]	Increased mass transfer in slag due to forced convection; realistic method(s) to simulate the actual situation in BOS converters.
Dynamic condition—sampling from industry converters	Sampling from industry converter ^[15,16]	2CaO–SiO ₂ (or 3CaO–SiO ₂) boundary layer at the lime particle–slag interface is moved away by dynamic stirring in converter, leading to lime dissolution mechanisms under varying dynamic conditions (Figure 1)
Direct observation	HT-CLSM observation of lime particle dissolution in slag; ^[17] X-ray radiography observation of slag penetration in lime ^[18]	Temperature and slag chemistry influence lime dissolution; slag penetration along the cracks in lime sample promotes lime dissolution

CaO–FeO–SiO₂ slag and lime cube sample. The other attempts to increase the convection include using a molybdenum impeller^[11] or an alumina impeller^[12] rotating at a certain speed to promote the agitation of the metal/slag bath. Maruoka et al.^[13,14] measured the dissolution rate under the experimental condition of argon gas bubbling through an iron tube into slag. In this method, the molten slag with lumpy lime added was stirred by argon gas bubbling, and the lime dissolution rate was calculated by monitoring the CaO concentration change in the slag. The authors believed that their technique is the most realistic method to simulate the actual situation in BOS converters.^[14]

Li et al.^[15] acknowledged that the understanding of the actual dissolution behavior of lime in an industrial furnace with vigorous stirring caused by oxygen jet impinging and slag–metal droplet reaction is poor. They studied the slagging behavior of lime in a 6 ton converter during the improving phosphorus refining (IMPHOS) project^[16] and a 320 ton industrial converter by directly sampling from the BOS converters, in comparison with slag samples taken from the hot-metal dephosphorization experiment using lime particle-containing slags in an induction furnace. In the 6 ton converter, slag was sampled several times after the start of blowing using a specially designed sampler system to obtain material from various depths within the slag bath. For the 320 ton converter, slag was sampled during slag tapping using a steel chain. For both cases, an interfacial layer of dicalcium silicate (C₂S: 2CaO · SiO₂) was not found at the interface between the undissolved lime particles and molten slag, whereas in laboratory static experiments^[2–5] and a hot-metal dephosphorization experiment^[15] this interfacial layer was detected and considered a kinetic barrier for lime dissolution in slag. They concluded that under the strong stirring condition within the industrial converter, the interfacial layer was actually mechanically removed and consequently the formation rate of this layer does not have an important role in lime dissolution.

Direct observation for lime dissolution into slag has been conducted using a high-temperature confocal laser scanning microscope (HT-CLSM)^[17] and direct X-ray observation of the slag penetration into a lime rod.^[18] In the former, the dissolution of lime particles in molten CaO–Al₂O₃–SiO₂-based slags was observed through HT-CLSM at temperatures between 1450 and 1600 °C. The dissolution behavior was found to be largely dependent on temperature and slag chemistry; that is, the lime dissolution rate considerably increased with increasing temperature, and addition of MgO into the CaO–Al₂O₃–SiO₂ slags promoted lime dissolution. In the latter,^[18] the phenomena of liquid slag penetration into solid bulk lime and into the cracks of the lime sample were investigated by in situ X-ray radiography direct observation by immersing the lime sample into CaO–SiO₂–Fe₂O–MgO molten slag at 1350, 1450, and 1550 °C.

2.2. Mechanisms of Lime Dissolution in BOS Slag

It is generally concluded from the lime–slag experiments under static conditions that when a solid lime sample is dipped into static slags, (Ca, Fe)O solid solution next to the lime particles and 2CaO · SiO₂ (or 3CaO · SiO₂) next to the slag will form at the lime–slag interface. The boundary layer formed at the interface between the lime particle and the liquid slag is considered a

kinetic barrier for lime dissolution in slag.^[2,3,6,17] Therefore, destructing the dicalcium silicate (C₂S) layer, the kinetic barrier, can promote the dissolution of lime in slag, which can be achieved by the stirring-promoted fluid flow and the formation of CO₂ inside the quick lime (e.g., uncalcined limestone core).^[14]

Examination of a slag sample taken from the hot-metal dephosphorization experiment described previously in the induction furnace confirmed, across the slag–lime particle boundary, the existence of two layers of a dense and continuous C₂S–C₃P (2CaO · SiO₂–3CaO · P₂O₅) solid solution layer next to the bulk slag and an FeO/MnO-rich layer next to the lime particle. However, no continuous C₂S–C₃P layer was observed for the slag samples taken from the 6 t pilot plant converter and the 320 t industrial converter.^[15]

By considering extensive research on lime dissolution so far, the present authors^[15] conclude the mechanism for lime dissolution in BOS slag as schematically shown in **Figure 1** under varying dynamic conditions. The dissolution of lime in slag is considered to be two-way diffusion (Figure 1a): outward diffusion of Ca²⁺ ion into slag and inward diffusion of slag components into lime. The inward diffusion is led by the faster diffusion of the ions of Fe²⁺, Mn²⁺, and Mg²⁺, resulting in the formation of an FeO/MnO/MgO-rich layer next to the lime particles and followed by the slower diffusion of anion complexes SiO₄⁴⁺ and PO₄³⁻ resulting in the formation of a C₂S–C₃P solid solution layer next to the slag (Figure 1b). The extremely dynamic conditions in the 6 t pilot plant converter and the 320 t industrial converter remove the boundary layer surrounding the “moving” lime particles with the possibility of the formation of a C₂S layer, which explains the difference in morphology across the lime–slag interface in the slag samples between the industrial converter and laboratory static experiment. Under strong convection such as within industrial converters, the retarding C₂S–C₃P solid solution layer at the lime–slag interface is removed and the slag bulk is homogenized (Figure 1c).

2.3. Modeling Lime Dissolution in BOS Slag

Modeling studies on the lime dissolution in BOS slag have been relatively fewer, and attempts have been made to develop a lime dissolution submodel for prediction of the slag composition and the resultant refining performance in the BOS process.^[19,20] Sarkar et al.^[19] argued that it is unlikely that a single mechanism will be rate-controlling throughout a real steelmaking process considering the fact that slag conditions such as basicity, FeO content, and temperature vary continuously during the blow. A mixed control model that takes into account contributions from all three kinetic steps would be more appropriate. The three kinetic steps involved in the dissolution process are: 1) diffusion of SiO₂ from bulk slag through a slag–C₂S boundary layer; 2) diffusion of SiO₂ through the C₂S layer; and 3) interfacial reaction between solid CaO and SiO₂ at the interface between unreacted CaO and the solid C₂S layer. It should be pointed out that the assumptions used in this modeling work contradict some facts observed in extensive experimental studies; i.e., 1) two way diffusion does exist in the lime dissolution, and in particular FeO and MnO diffuse much faster than SiO₂ and outward diffusion of CaO, and 2) no C₂S layer was found to exist around lime particles

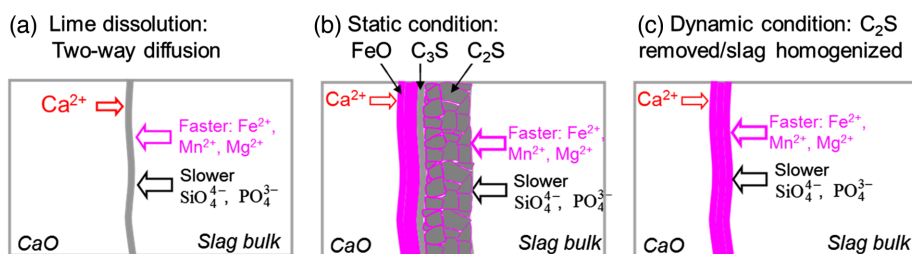


Figure 1. a–c) Schematic diagrams showing the mechanisms of lime dissolution in slag under varying dynamic conditions.

in the forced convection experiments and in the slag samples from industrial converters. Dogan et al.^[20] developed models for lime and dolomite dissolution as a function of temperature, slag composition, and stirring intensity for BOS slags at high temperatures. They considered that the lime dissolution rate is assumed to be controlled by CaO diffusion through a boundary C₂S layer. They also noted from the literature that the C₂S film layer disappears under forced-convection conditions and the formation of (Fe, Mg)O (i.e., an FeO/MgO-rich layer) is hardly affected by the intensity of stirring, and therefore, they introduced a parameter for stirring intensity due to the CO generation in the BOS process. They concluded that the flow rate of the stirring gas has a crucial impact on the rate of dissolution of flux additions. Their model could be more applicable to industrial conditions.

2.4. Effect of Slag Composition on Lime Dissolution

In the early stage of the BOS process, the BOS slag mainly consists of FeO and SiO₂, resulting from the oxidation of Si and Fe in hot metal. With the dissolution of fluxes (lime, dolomite) and continuous oxidation of other elements (such as Mn, P) in the hot metal, the BOS slag evolves into a multicomponent CaO–SiO₂–FeO–MnO–Al₂O₃–MgO–P₂O₅ system. The FeO content in the BOS slag varies from ≈50 wt% in the early stage through low FeO content in the middle of blow to 15–25 wt% at the end of the blow (depending on the steel products and blowing practice). Considering the slag composition in the BOS process, FeO-containing slag should be selected to study the lime dissolution. FeO (as well as MnO and MgO) can promote the dissolution of lime in the slag because of their faster diffusion from slag to lime (Figure 1a). This is evident by the formation of a (Ca, Fe, Mn, Mg)O FeO/MnO/MgO-rich layer in the lime side at the lime–slag interface.^[5,6,15] Further evidence is the dissolution rate into FeO-containing slags being several times greater than that into slags without FeO.^[6] Even in static experiments it is found that the 2CaO·SiO₂ layer in slags containing high FeO and low SiO₂ contents is discontinuous and has a smaller retarding effect on the dissolution of the lime, whereas the dense 2CaO·SiO₂ films are formed continuously in slags containing low FeO and high SiO₂ contents, and would retard the dissolution rate markedly.^[6] MnO_x has a similar effect on lime dissolution to that of FeO.^[7] The results on the effect of MgO in slag are contradictory as Guo et al.^[17] reported that the addition of MgO in CaO–Al₂O₃–SiO₂ slags is beneficial for lime dissolution, whereas Cheremisina et al.^[5] found that MgO (4.3–7.6%) in steelmaking CaO–SiO₂–FeO slags hinders the process of CaO dissolution and slows down the rate

of dissolution of lime samples. It should be pointed out that the CaO–SiO₂–FeO slags tested by Cheremisina et al.^[5] are more applicable to the BOS process.

As shown in Figure 1, SiO₂ has a negative effect on lime dissolution due to its reaction with CaO to form 2CaO·SiO₂ and/or 3CaO·SiO₂. This is evidenced by experimental results from various researchers.^[6,7]

Addition of CaF₂ and TiO₂ to the slag was reported to increase the CaO diffusivity.^[7] In particular, addition of CaF₂ had the strongest effect and increased the diffusivity by a factor of 3 to 5 at temperatures between 1500 and 1600 °C.^[7] However, Nowadays CaF₂ is rarely used in the BOS process due to environmental concerns.

Other factors may include basicity (CaO/SiO₂) and viscosity.^[21] The CaO diffusion rate in slag decreases with increasing slag viscosity and this is influenced by the structure of the liquid phase and solid fraction in slag, which suggest the existence of an optimum basicity for effective CaO dissolution. The dissolution of lime increases the slag basicity and a lower viscosity of the slag is obtained, which enhance the dephosphorization process, whereas a very acidic slag would increase the size of the silicate anions and consequently the viscosity, resulting in the decreased foaming ability of the slag.^[11]

2.5. Lime Properties

The reactivity of lime is considered to be a key index reflecting the ability of lime to dissolve in steelmaking slags. The reactivity of lime is measured by reacting lime with water or acids (e.g., hydrochloric acid, HCl) at ambient temperatures according to relevant standards such as the European standard EN 459-2. Such a test can only provide an indication of the ability of the lime to react with the slag because of the following two reasons. First, the steelmaking temperature for lime dissolution in BOS slag is significantly higher than the ambient temperature that the reactivity of lime is tested at. Second, the BOS slag is an ionic solution at steelmaking temperatures and thus behaves differently to water. It has been an unsolved challenge to develop a suitable high-temperature method to evaluate the reactivity of lime with steelmaking slags. A reactive lime has small crystals and high porosity.^[22] The reactivity of lime varies with the quality of the limestone (e.g., the amount of impurities, its texture) and calcination practice. Overburnt lime usually has reduced porosity and reactivity, whereas a high-reactivity lime often has an unburnt carbonate located at the lime center.

The lime charged into top-blown converters is in the size range of 5–60 mm. The smaller particle size favors a larger area of specific contact with the slag, which increases the lime dissolution rate.^[12] However, more than 80% of lime particles less than 5 mm in size escape into off-gas systems.

For the convenience of experimental research, dense lime (often pre-fused or sintered) samples (such as rod, disk) are used in the rotating experiments for lime dissolution. However, quick lime (porous and at the lowest level of calcination) is used in the BOS operation. The simultaneous penetration of slag into the pores in quick lime significantly promotes the dissolution of lime in BOS slags.^[6,15,18]

2.6. A Brief Summary for Lime Dissolution

Experimental research on the lime dissolution in BOS slags has been extensively conducted by various means, from static conditions through rotating disc/rod and forced convection to directly taking slag samples from BOS converters. The understanding of lime dissolution mechanisms has been well advanced, which is schematically shown in Figure 1. Some recent experimental methods could generate improved outcomes; however, further scientific evidence should be provided to prove their similarity with industrial converters in terms of dynamic conditions. Modeling work on lime dissolution in BOS slags is underdeveloped, and the advanced understanding of lime dissolution could help develop a better lime dissolution model for prediction of slag composition and better BOS process control. It has been an unsolved challenge to develop a suitable high-temperature method to evaluate the reactivity of lime with steelmaking slags as the reactivity of lime tested by reacting lime with water or acid at ambient temperatures can only give indication of its dissolution in slag at high temperatures.

3. Real Time In Situ Diffraction on High-Temperature Behavior of BOS-Type Slag

3.1. BOS Slag for Phosphorus Refining

One of the key challenges in the BOS process is to efficiently remove the impurity phosphorus from the hot metal to the BOS slag. Hot-metal dephosphorization is primarily driven by the refining of droplets in the slag–metal emulsion zone (the slag–metal droplet reactions are studied in Section 4), and more than 90% of dephosphorization is achieved by the slag–metal droplet reaction.^[23] There is an increasing demand to fully understand the high-temperature behaviors of BOS slags for the purpose of accelerating phosphorus removal. Extensive research has been conducted to study the high-temperature behavior of BOS slags by experimental research and thermodynamic simulation in relation to phosphorus removal.

The BOS slag is generally perceived in the solid–liquid coexisting state at steelmaking temperatures ($\approx 1650^\circ\text{C}$), initially for the purpose of minimizing the refractory erosion. Lately it has been known that phosphorus dissolves into the $2\text{CaO}\cdot\text{SiO}_2$ phase as $3\text{CaO}\cdot\text{P}_2\text{O}_5$ ^[24] and is present in the BOS slag as a $2\text{CaO}\cdot\text{SiO}_2\text{--}3\text{CaO}\cdot\text{P}_2\text{O}_5$ ($\text{C}_2\text{S}\text{--}\text{C}_3\text{P}$) solid solution.^[25] Extensive research has been performed to adjust the slag

composition and the solid phases for improving the phosphorus refining performance in the BOS process over the past two decades, focusing on the phosphorus partition between $2\text{CaO}\cdot\text{SiO}_2$ particles and $\text{CaO}\text{--}\text{SiO}_2\text{--}\text{Fe}_t\text{O}$ slags and the mechanism of dephosphorization with $\text{CaO}\text{--}\text{SiO}_2\text{--}\text{Fe}_t\text{O}$ slags containing mesoscopic-scale $2\text{CaO}\cdot\text{SiO}_2$ particles.^[26–33] This research has significantly advanced the understanding of the high-temperature behavior of BOS slags, including their heterogeneous nature and their reaction with phosphorus.

Most experimental researches have been conducted for the naturally cooled and or “quenched” slag samples taken from laboratory experiments and pilot-scale and industrial converters. With these methods, it is not possible to determine if certain phases observed in the samples at ambient temperature exist at the steelmaking temperatures or form only upon sample cooling. Thermodynamic simulation using carefully developed thermodynamic databases and packages (either commercially available or in-house developed) can predict different thermodynamic aspects of phosphorus-containing steelmaking slags in the composition, temperature, and oxygen partial pressure relevant for the industry processes.^[33,34] However, the validation of simulation result is a challenge due to the lack of high-temperature experimental results of multicomponent slags. Therefore, direct observation of the BOS slag behaviors at steelmaking temperatures can help advance the understanding of the high-temperature behaviors of BOS slag and validate thermodynamic modeling results.

3.2. Real Time In Situ Diffraction on High-Temperature Behavior of BOS-Type Slags

To understand the phase transformation of BOS-type slags (multicomponent oxide systems) upon heating and cooling, Li et al.^[35] conducted real-time in situ neutron diffraction study of the high-temperature behaviors of synthetic BOS slags as a function of composition, temperature (up to 1700°C), and time. It was aimed to clarify the phase conditions of the BOS-type slags as a function of composition and temperature, advance the understanding of the phosphorus refining process in the BOS process, and provide valuable information for the development of thermodynamic packages of the multicomponent oxide system at high temperatures.

The behaviors of synthetic BOS slags at high temperatures up to 1700°C were studied by developing a real-time in situ neutron diffraction method on the General Material diffractometer (GEM) of the spallation neutron source at the ISIS Neutron and Muon Source, Rutherford Appleton Laboratory, UK. GEM is a high-resolution powder diffractometer with penetration depth of several centimeters.^[36] It can measure both crystalline-phase materials and liquid samples and is sensitive to subtle phase transitions. GEM has detector arrays containing about 7000 individual detectors, covering forward and backscattering angles, which gives the advantages of rapid data collection of a neutron pattern.

The phases present in the sample under the neutron diffraction experiments were determined (indexed) by search match using the X-ray powder diffraction file (JCPDS) and the neutron diffraction data collected for the BOS slags. A “thermohistogram” (Figure 2) can be useful for the purpose of indexing,

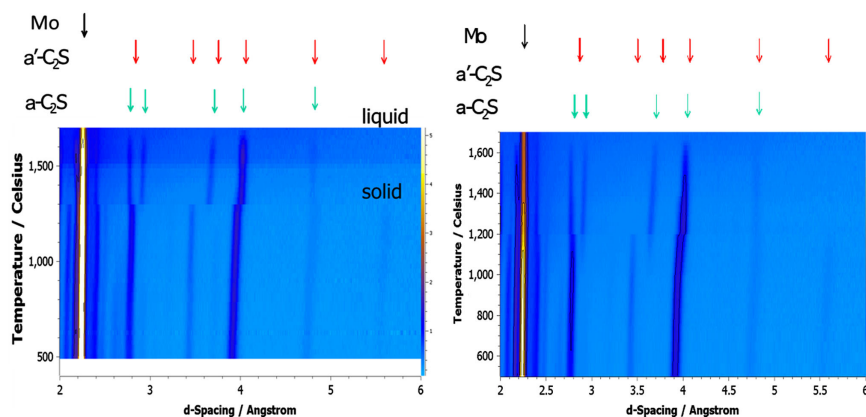


Figure 2. Phase evolution of a synthetic BOS slag (sample C: CaO–SiO₂–FeO–3%MnO–1.5%Al₂O₃–6%MgO, CaO/SiO₂ = 2.5, and FeO = 20%) during heating (left) and cooling (right). Mo: molybdenum crucible.

in which a plot of diffraction patterns for a sequence of temperatures indicates Bragg reflections as color trace, indicating the expansion behavior of the phase (bent line) and phase transformations. The color scheme indicates the count rate for a particular *d*-spacing and temperature.

Quantitative phase analysis, assessing the amount of each phase in the sample either as volume or weight fractions was conducted by full-pattern Rietveld refinement.^[37,38]

As shown in **Figure 3**, for the slag sample C (CaO/SiO₂ = 2.5), which is close to actual BOS slag, the main phases in the temperature range of 500–1700 °C detected by the neutron diffraction are α-C₂S, α'-C₂S, halilite (CaO/FeO/MnO/MgO), hatrurite (C₃S), β-C₂S, γ-C₂S, and srebrodokitite (Ca₂Fe₂O₅). The slag was observed to melt at ≈1700 °C, which indicates that the BOS slag at steelmaking temperatures (≈1650 °C) is likely to be a mixture of solid and liquid phases. The dominant phase is α-C₂S at high temperature and α'-C₂S at low temperature. The abrupt phase transformation temperature between α-C₂S and α'-C₂S is between 1200 and 1300 °C. Hatrurite (C₃S) was detected during both heating and cooling. It was also found that difference between this in situ observation and thermodynamic calculation does exist in terms of melting temperature and phases (e.g., C₃S phase).

3.3. A Brief Summary for Neutron Diffraction

A real-time in situ neutron diffraction study up to 1700 °C was conducted for synthetic BOS-type slags in a specifically designed experimental setup and procedure on GEM at ISIS Neutron and Muon Source, UK. Relative phase fractions and structure parameters of the phases present in the slag samples studied were obtained by analyzing the collected neutron diffraction data as a function of composition and temperature. It clearly indicates that the in situ neutron diffraction method developed here can be used to study the high-temperature behavior, particularly the phase transformations upon heating and cooling, of metallurgical slags as a function of composition, temperature, and time. A solid dicalcium silicate (C₂S) phase was detected to exist in the synthetic BOS slag at steelmaking temperatures up to 1700 °C, which implies that the BOS slag at steelmaking temperatures (≈1650 °C) is likely to be a mixture of solid (e.g., C₂S) and liquid phases. The slag phases during heating and cooling varied with the slag compositions. The slag phases detected by the in situ neutron diffraction were found not to completely agree with thermodynamic package prediction, which could be an interesting topic for future research.

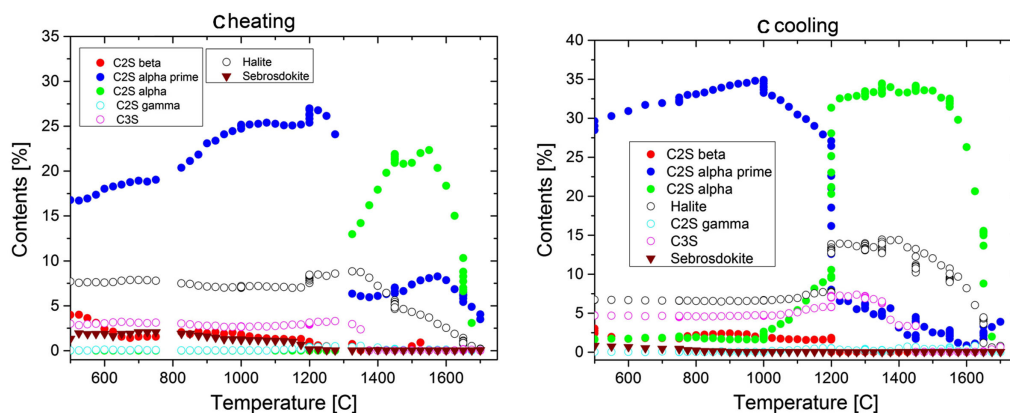


Figure 3. Phase evolution for slag sample C during heating (left) and cooling (right) detected by neutron diffraction study.

4. Transition Phenomena in BOS Slags

The influence of the gas/slag/metal emulsion within the BOS converter as a major contributor to refining rates due to the cumulative interfacial area of metal droplets is a concept agreed upon by a plethora of academics and industrialists.^[39–47] In addition contributing to the primary function of the vessel, decarburization (Equation 1),^[44,48,49] the emulsion is also a dominant contributor to the control of phosphorus levels (Equation 2).^[23,50] The contribution of the emulsion varies with time during the blow, which, along with the specific reaction rates due to the chemical environment, is largely thought to be controlled by the population, size, and shape of the metal droplets within the emulsion at a given time.^[16,51]



where species within square brackets [] are in the metallic phase, and species within round brackets () are within the slag phase.

4.1. Potential Contribution of Droplets in the BOS Emulsion

There have been two major methodologies used to explore the macroscopics of droplet populations in BOS emulsions. These include pilot scale sampling and measurement of a furnace either during continuous processing or interrupted trials, and mathematical modeling approaches applied to fundamental observations of droplet formation and reaction kinetic controlled mobility. These methods have been used to calculate the overall refining potential of the emulsion zone to decarburization, dephosphorization, and other reaction profiles within the converter. The amount of metal, the time it exists within the emulsion for, and the rate at which it moves are all considered. A mass balance approach to calculating these macro emulsion variables was taken by the current authors with extensive data published across multiple pilot scale trials.^[52] The general trends were found to show metal volumes peaking between 4 and 6 min, residence times reached their highest of up to 120 s around mid-blow (8 min), and metal circulation rates steadily rose through the blow before an exponential increase at the end blow, which was rationalized due to foaming reduction and droplets moving through gas rather than a sustained emulsion.

The macroscopic findings were compared against previous experimental trials^[53] as well as an extensive study conducted by academics using first-principles reaction kinetics and modeled droplet generation understanding.^[46,54–59] Overall, the two approaches showed good correlation with complementary understanding uncovered to give credence and mutual reinforcement of the findings. It was found that dependant on blow time the emulsion could contribute over 60% of the overall decarburization rate of the BOS converter and a greater proportion of reactions which require the slag phase for product partitioning (such as silicon, phosphorus, manganese, and chromium removal).

Table 2 gives a summary of the findings on droplet size presented within the literature from pilot scale sampling. The variance is considerable and is not correlated against the in situ or

stop–start-based approaches taken. As such, it is expected that this variance depends more on the cooling rate of the samples taken, with slower cooling having given time for droplets to coalesce, reducing their number and reducing the cumulative surface area but increasing the droplet size recorded.

The present authors have worked on the measurement of quenched samples taken during in situ sampling from a pilot scale BOS converter.^[16] The methodology of the sample collection has been reported in detail previously and was part of the European Commission project IMPHOS: improved phosphorus refining.^[16] Fragments of the samples taken from nearest the sample pot wall (and thus cooled the fastest due to direct contact with the “cold” mild steel of the sampling pots) were subjected to investigation via 3D X-ray computed tomography (XCT). This methodology allowed the full volume of the spheres to be detected, unlike the cross-sections which are relied upon to be representative in previous studies, as well as a greater number of droplets to be measured accurately and while in contact with the slag phase of the emulsion due to the nondestructive nature of the characterization technique.

Figure 4 gives an example 3D volume of a sample that was reconstructed from an XCT scan. The image displays several shards that were scanned together while mounted in epoxy to hold them in place. The variation in metal droplet size, population density, and morphology can be seen to vary to a significant extent across the samples. The rigor of interrogation that this sample methodology gives allows for a quantified accurate understanding of the metal droplets found within the BOS emulsion.

A selection of samples was interrogated across both the time of BOS blow and height within the emulsion. It was found that the number of droplets detected for similar sized samples at the same height in the converter (≈ 0.5 m above the quiescent bath interface) ranged from at its lowest 560 droplets at 12 min into the blow to 11 996 droplets at 16 min (almost end of the blow), as well as between 1062 at the lowest sampling level (within 25 cm of the bath interface) to 134 at the highest sampling point (≈ 1.5 m above the quiescent bath interface).

As well as divulging the variance in droplet number and size, the findings also allowed interrogation of the individual droplet morphologies. Figure 5 shows a higher magnification XCT reconstruction of some droplets found within an emulsion sample. Within the image, the individual metal droplets are easily seen through color coding. Two distinct droplet morphology types can be considered from this image: 1) droplets that are seen to be mostly spherical, with potential smooth building or bloating, and 2) droplets with highly divergent topologies away from spherical, where rough “growth” or dispersion of the droplet is seen—microemulsions. These two different morphologies are considered to be the result of gaseous product reaction in the case of bloating and liquid state material transfer in the case of microemulsions.

With these droplets in close proximity, it would be a fair assumption that the slag phase is of similar composition and the environment has similar physical conditions. As such, it is thought that the composition of the droplets themselves is dictating the alternative behaviors, with those displaying bloating behavior undergoing significant decarburization, generating internal gas fractions to the droplet, and those displaying microemulsion behaviors undergoing dominant reaction such as

Table 2. A summary of the experimental approaches to investigating metal droplet size in the BOS gas–slag–metal emulsion. Reproduced under the terms of the Creative Commons CC-BY license.^[95] 2016, Springer Nature.

Researchers	Place of collection	Droplet size range [μm]
IMPHOS ^[16]	Inside pilot converter, special lance	16–6360
Resch ^[144]	Paused and tilted converter	50–2000
Tokovoi et al. ^[145]	Upper slag/metal emulsion	1000–2500
Cicutti ^[53]	Inside full converter, special lance	230–3350
Koria et al. ^[146]	Slashed liquid outside crucible	40–70 000
Baptizmanskii et al. ^[147]	Cutting hole in crucible wall	50–18 000
Meyer ^[148]	Through tap hole, outside converter	150–3320
Block et al. ^[149]	50–150 mm above bulk bath inside converter	500–4000
Urquhart et al. ^[150]	Inside full converter, special lance	63–2000

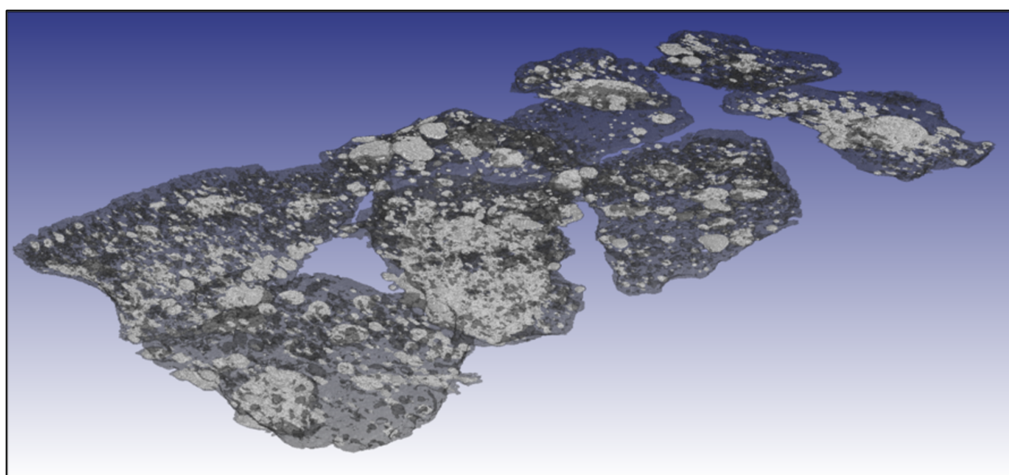


Figure 4. A 3D reconstructed image of quenched fragments of material taken from the emulsion zone of a pilot plant BOS converter.^[16] The slag phase has been made to appear semitransparent (medium gray), allowing the observation of metallic droplets (light gray) and porosity (dark gray) that were captured within the samples during solidification.

dephosphorization after carbon levels within the droplet have already been depleted and thus oxygen from the slag phase is able to react with species other than carbon at a greater rate. The following sections will discuss these phenomena in greater detail through the use of laboratory techniques.

4.2. Decarburization-Driven Bloated Droplets

As stated previously, decarburization is the primary function of the BOS process, with hot metal entering the vessel generally at over 4 wt% carbon and products generally requiring less than 0.1 wt% carbon. This equates to (for a 300 tonne converter) over 8 tonnes of carbon removal required over the 18 min of an average vessel in operation.

Several groups have built specialized equipment and combined powerful techniques to investigate the decarburization of individual droplets. Molloseau and Fruehan^[60] and Coley et al.^[61–64] have published a plethora of studies making use of X-ray radiography techniques combined with a vertical tube furnace. These researchers have made observations on the effects

of carbon content, iron oxide, sulfur, temperature, and other parameters on the rate of decarburization that a single metallic droplet undergoes. Through the direct observation techniques, phenomena such as gas halo formation and droplet bloating,^[65,66] rising and falling again have been observed. The observation of these phenomena was key to unlocking the understanding of droplet residence time within the BOS converter. Brooks originally calculated that with the velocity and trajectory of a droplet on leaving the bulk bath surface, a droplet would stay “airborne” for less than 2 s,^[67] which would cause circulation rates close to those reported by the current authors at the end blow. However, with the addition of understanding on bloated droplets effective density reduction and the ability for the slag phase to suspend the more buoyant droplets for extended periods of time,^[39,68,69] the realization that droplets could indeed exist for extended periods within the emulsion and reach near-equilibrium levels of reaction condition blazed the pathway for the modern understanding of the BOS emulsion.

The present authors conducted experiments using a small IR furnace placed within an XCT scanner. The furnace heated the sample rapidly to the target experimental temperature of

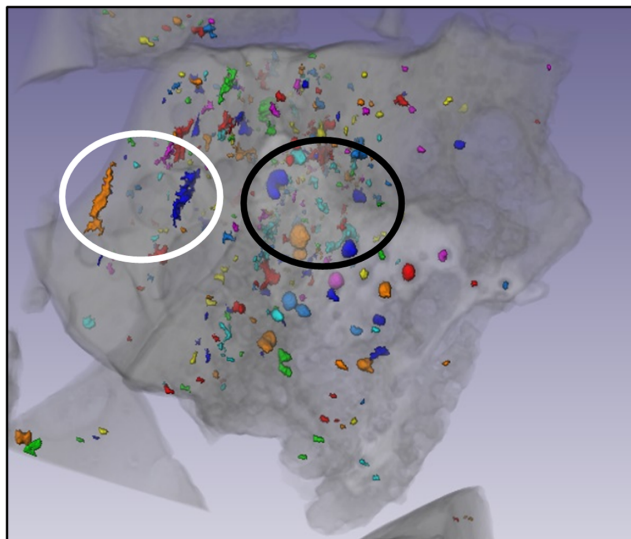


Figure 5. A high-magnification XCT reconstruction of a quenched BOS emulsion sample. The slag phase has been made semitransparent (light gray) for internal metal droplets to be visualized (segmented with a range of colors). Key droplets displaying bloating behaviors (blue and orange droplets are easiest seen) are seen within the black circle, and key droplets displaying microemulsification behavior (orange and blue) are seen within the white circle.

1600 °C, while the XCT scanner conducted limited-angle tomography to enable rapid imaging of the sample held within the furnace. This technique allowed for higher-resolution imaging of the droplet in situ while undergoing decarburization at reaction temperatures.^[70]

Figure 6 displays a series of top-down images of a sample crucible with the time increasing from left to right. Within the images a pore is seen to develop due to the formation of carbon dioxide, and it is acutely seen to grow before moving to the droplet surface and escaping. This porosity formation and ejection from the droplet is considered to show in detail the pathway of bloated droplets occurring, and the oscillation effects of density that were observed by previous studies.

The details of this study are awaiting alternative publication; however, the authors were able to quantify time periods of gas porosity formation, ejection, and reformation via this method. As well as the overall time period, a given sample system continued to develop internal porosity. As well as internal porosity, where carbon levels were lower interfacial gas phases were seen to be dominant in the form of a gas halo, which gradually leaked away from the droplet. This again confirms in detail the finding of earlier studies with the output being an understanding of when a shift from one behavior to another occurs.

With regard to application within the BOS converter process itself, the difference between internally and externally generated gases is significant. The BOS is a highly dynamic process with droplet environments subject to significant turbulence and the overall circulation rate.^[71–74] It is thought that when gaseous products are generated internally to the droplet this will contribute to the reduction of the effective droplet density with much greater effect, as compared to a gas halo, which could be

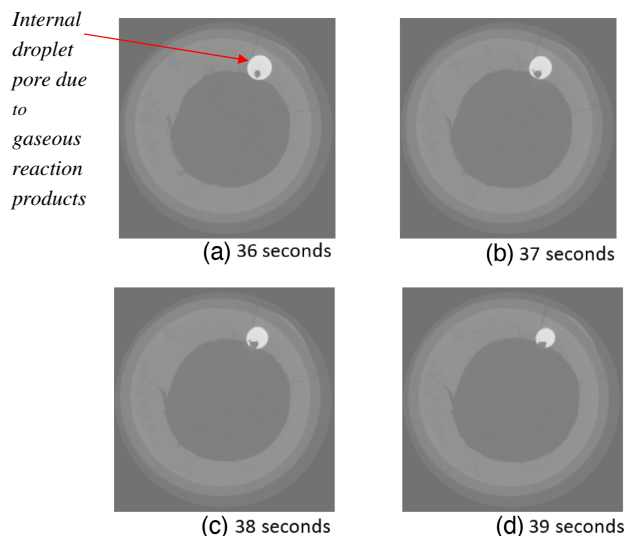


Figure 6. a–d) A time sequence of top-down images captured in-situ during the decarburization of a metal droplet through reaction with FeO in the slag phase via limited angle XCT. The droplet is seen in white, the slag in light gray, and voids in dark gray. The large center-circle void of the image is due to the horizontal cross-section of the image through the sample intersecting the meniscus layer (i.e., the center of the image is above the slag layer, whereas the sides are within the higher parts of the upward-curved meniscus).

disrupted by slag movement. The chemical conditions that cause internal porosity generation to form correspond to those where highest residence times and decarburization are observed and/or calculated for the emulsion supporting this theory.

4.3. Spontaneous Emulsification of Metal Droplets

The overall refining rate of the BOS emulsion is a balance between the available reaction area and the time for which the material is in contact. The previously discussed phenomena of bloated droplets contribute to the time that a given droplet is suspended for and thus enable longer reaction times. However, after decarburization reduces, this phenomenon is expected to drop off quickly. Despite this, elevated levels of refining are still seen for other impurities, such as phosphorus,^[75–78] well beyond what would be possible from the interaction of a quiescent surface alone.

From the study that contributed to the previous discussion on the macroscopic dynamics, the authors were able to measure the average surface area to volume ratio of a droplet through the blow of the pilot BOS converter. These are shown in **Table 3**. There is a clear significant rise in the surface area to volume ratio around 10 min into the blow. At this time, decarburization rates are

Table 3. The average surface area to volume ratio of XCT measured metal droplets at different times during a BOS blow.

Blow time [min]	2	4	6	8	10	12	14	16
Average SA/vol	56.57	49.66	0.20	37.78	217.50	123.40	22.83	61.56

moderate, with carbon levels within the metal recorded at being around 1 wt% C. Previously reported findings in the literature show that a droplet would reach near-equilibrium levels of carbon within the residence times calculated for droplets at this time,^[61,79,80] meaning gas generation would be reduced around the droplet, allowing a continuous slag/metal interface.

The highlighted droplets with complex morphologies within Figure 5 would have very high surface area to volume ratios compared to more spherical droplets whose shape would be dictated through surface area minimization energetics and only increase linearly through bloated-droplet phenomena.

Previous researches, including key contributions to the literature by Riboud and Lucas^[81] and Rhamdhani et al.,^[82–84] have investigated the reaction of a single metal droplet with a BOS-type slag. These authors used methodologies such as quenching and then separating the metal and slag phase before applying paper coverage or similar techniques to measure the surface area of recovered droplets. These authors recovered multiple smaller droplets from their trials when only a single larger droplet was placed within the sample to begin with. The conclusion is the droplets had broken apart during the experiment. Many authors have explored the effect of chemical reaction on the interfacial tension between the liquid metal and slag, with the high levels of reaction, oxygen, and sulfur all contributing to the reduced surface area.^[85–92]

The present authors have conducted multiple studies through the use of rapid heating and quenching in a high-temperature confocal scanning laser microscope, which has been coupled with both in situ visualization of the droplet when a transparent slag was used,^[93,94] and XCT investigation of the quenched samples when direct observation was not possible, and quantified the surface area desired.

Figure 7 shows a time sequence of 3D-XCT-reconstructed quenched samples from a system containing high-purity iron droplets and a slag phase with over 35 wt% FeO. The droplet is seen to perturb away from a smooth sphere before breaking apart into a cloud of material at 90 s—well within the calculated residence times possible in the BOS process.

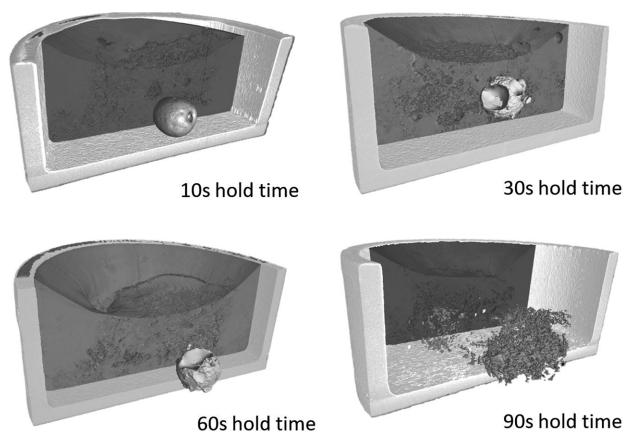


Figure 7. Time-step images of a metal droplet reconstructed from XCT-scanned quenched samples. The crucible and slag have been peeled back to reveal the droplet, which can be seen as a near-spherical object at 10, 30, and 60 s, but as a cloud of material at 90 s. Reproduced under the terms of the Creative Commons CC BY license.^[95] Copyright 2016, Springer Nature.

Comparing the high-resolution image of 90 s in Figure 7 with the droplet geometries within the white circle of Figure 5, there are significant similarities and thus the understanding of what causes this phenomena can be interrogated. The present authors have published multiple articles exploring the effects of chemical potential on the geometry of liquid metal droplets and have observed spontaneous emulsification for multiple systems.^[95,96] The fundamental pathway of perturbation formation, growth, necking, and budding has been quantified and modeled via phase-field methods to confirm that the understanding for the drive is fundamentally correct.^[97]

By significantly increasing the effective surface area of the droplets, and simultaneously reducing the droplet size to cause longer residence times (as turbulence within the emulsion will dictate droplet movement more than initial trajectory and gravity) spontaneous emulsification greatly increases the refining potential of the metallic phase within the emulsion and enables its overall contribution toward BOS refining.

4.4. Summary of Transition Phenomena in BOS Slags

In this section we have discussed the understanding of the macroscopics of the gas/slag/metal emulsion within the BOS converter, as well as individual droplet behaviors that have been observed by multiple research groups.

The combination of these findings is a powerful tool to enable process models to understand the refining driving force at a given point within the converter process, and the engineering of parameters such as metal droplet population and environments to improve refining performance. A key example of investigation would be applying the collective understanding to the issue of phosphorus reversion, which is seen within the converter at times.

In addition to the understanding these tolls give for BOF refining, there are many other processes within steel processing where discrete heterogeneous liquid phases are entrained within the other. Examples include during alternative ironmaking, steelmaking pretreatments, secondary steelmaking, and the inversion of the phases in situations such as mold slag entrainment within the liquid steel during casting (which has recently been reported to show the potential for similar phenomena to occur as steel grades continually develop to meet product demands of the future).

5. Energy and Material Recovery from BOS Slags

BOS slags, after completing their functions in the BOS process, are tipped out of the BOS converter and considered to be wastes or byproducts of the steelmaking process. BOS slags contain sensible heat (or thermal energy) because of their high temperature up to 1700 °C, chemical energy (e.g., metal droplet, low-valence metal ions), and valuable materials (metallic, metal oxides such as Fe_xO and MnO). Recovering the energy and materials encompassed in BOS slags has always been challenging but it is essential to increase the resource efficiency and reduce the environmental impact of steel manufacturing processes. This section reviews the recent progress in energy and material recovery from BOS slags. A novel process to recover energy and

materials from BOS slags developed by the present authors will also be briefly introduced.

5.1. Energy Recovery

Effectively utilizing the huge amount of waste heat produced by steelworks is an important challenge with great potential to save energy and reduce CO₂ emissions. On cooling slags from 1500 °C to ambient temperature about 1.8 GJ of thermal energy could be released from each tonne of blast furnace ironmaking slag. In this section, we will first review the state of the art of energy recovery from metallurgical slags, including blast furnace ironmaking slags.^[98]

5.1.1. Heat Recovery by Hot Air/Steam via Granulation

To recover the heat in blast furnace slag, an air-blast-based process was researched in the 1980s as a national project in Japan.^[99–106] In this new approach, molten slag is atomized under centrifugal forces on a spinning disc, to produce fine droplets, which are quenched by air to produce glassy granules suitable for cement production. This dry slag granulation (DSG) process also produces hot air of 500–600 °C for on-site utilization such as drying, preheating, steam or electricity generation, or other suitable applications. Recently, a new bench-scale slag heat recovery system was developed under the Japanese national program COURSE50 with the targets of obtaining the hot gas exchanged by hot slag with temperature above 140 °C and achieving a heat recovery ratio of above 30% versus 1450 °C molten slag.^[107] In this process, the molten slag is solidified on the surface of two water-cooled rolls and conveyed to a slag heat recovery chamber, where ventilation by two blowers is achieved and consequently the hot air is obtained by transferring the slag thermal energy to the blown air. Another trial to recover waste heat of the blast furnace slag in the form of sensible heat of hot water after wet granulation has also been reported.^[108] In this wet granulation process, the molten slag is treated conventionally by impinging it with a large amount of water for the granulation and glassifying processes. It is worth noting that water granulation of slags is associated with minor air pollution through emission of sulfur-containing gases to the atmosphere. Water granulation consumes considerable volume of fresh water and does not allow recovery of high-grade waste heat from molten slag.

The recovery of sensible heat in slags by the granulation method has been widely developed and gradually adopted by the industry for blast furnace slags. It greatly contributes to the efficient recovery of waste heat from molten blast furnace slags while generating high-quality glassy materials for other industries such as cement. Attempts to apply granulation methods to BOS slags have been proven extremely challenging as the chemistry and physicochemical properties of BOS slags differ greatly from those of blast furnace slags. Furthermore, the chemical energy contained in BOS slags, i.e., metallic iron, iron oxides, and manganese oxides, cannot be recovered by the slag granulation methods. Research is required to effectively recover the waste energy contained in the high-temperature BOS slags.

5.1.2. Heat Recovery as Chemical Energy via Endothermic Reaction

Another route to recover the heat in molten slags is to convert the waste heat (thermal energy and or chemical energy) in the molten slags to chemical energy (e.g., syngas) via endothermic reactions. Some of the processes developed^[109–115] are summarized in **Figure 8**.

A novel process consisting of dry slag granulation and endothermic reaction between reactive gases and granulated slag particles has been reported^[109–115] that provides the possibility to recover the sensible and chemical energy in molten slag at a temperature over 1773 K. In the process, a rotary cup atomizer (RCA) can granulate molten slag from the blast furnace and BOS converter by centrifugal force and the slag granule is directly cooled by endothermic reactions of methane steam reforming. The reactive gases of methane and steam and the hot slag droplets move in a counter current through the moving bed and the preheated methane and steam are converted into hydrogen and carbon monoxide with the aid of a Ni-based material catalyst at the bottom of the RCA.

Another similar technique, containing molten slag granulation by a rotary multinozzle cup atomizer (RMCA) and pyrolyzing printed circuit board (PCB) with granulated slag particle, was proposed and verified by Qin et al.^[116–118] to recover the large amount of sensible heat in molten slag. The molten slag was first granulated by a rotary multi-nozzle cup atomizer. Then the hot granulated slag particles were used to preheat and pyrolyze the waste PCB powder into combustible gases by converting the energy of hot slag particles to chemical energy via the endothermic reactions. During the PCB pyrolysis reaction, a large amount of combustible gases such as CO, H₂, C_mH_n, and CH₄ was produced, which can be injected into the blast furnace to partially replace coke for reducing CO₂ emissions. In addition to the recovery of the energy in molten slag, the pyrolysis residual produced was separated from the slag particles to extract precious metals, and then the slag particle was used to produce cement. However, some issues, such as achieving high pyrolysis reaction rates, heat exchange, and the formation of HBr, need to be further investigated before the method can be put into practice.

An alternative method has been invented by Tata Steel Limited^[119,120] for producing syngas without carbon footprints. This novel technology uses the thermal energy of molten BOS slag or molten ferroalloy slags to generate hydrogen-rich gas (syngas). The principle of the hydrogen-harvesting method is based on thermochemical decomposition of steam on the surface of molten BOS slag. When water is sprayed on the molten slag, water vaporizes into steam while coming in contact with the slag surface due to the intense heat emitted from the molten slag. The molten slag contains metal oxides, such as Fe_xO, Cr_xO, and MnO, and metallic particles (Fe, Cr, Mn, etc) depending on the process. Thermochemical decomposition of steam takes place on the slag surface by reaction of steam with the metal oxides and the metallic particles present in the slag. Oxygen is trapped in the slag and hydrogen is released as the product gas. The technology thus utilizes the thermal and chemical energy of molten slag to produce hydrogen-rich gas that can be further purified to high-purity hydrogen. The technology

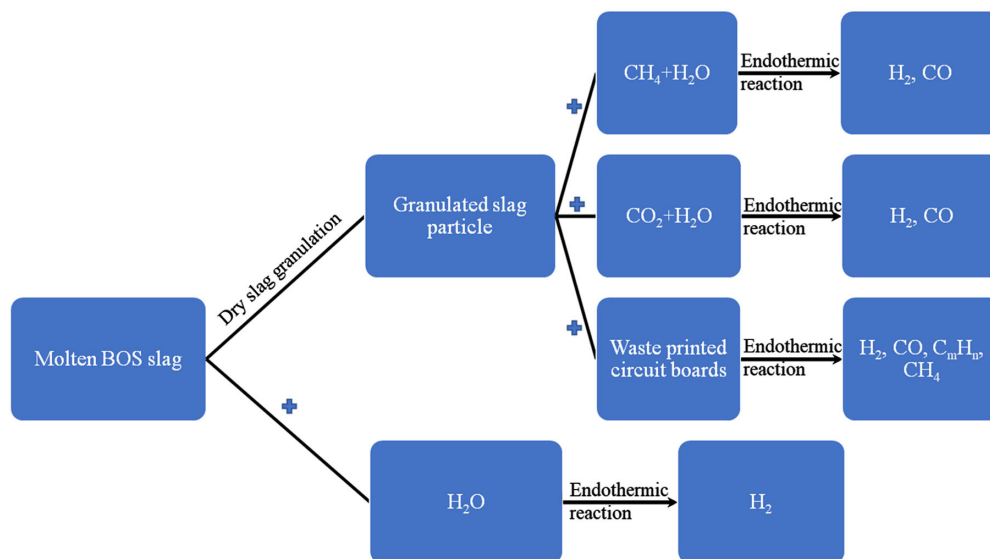


Figure 8. Schematic diagram for heat recovery from molten slags as chemical energy via endothermic reaction.

was first tested in laboratory experiments by spraying a limited quantity of water on molten steelmaking slag. The product gas was collected and subsequently separated from steam. Converting the concept from laboratory scale into industrial process provided some challenges such as understanding the factors affecting the generation behavior of hydrogen, exposing an active or fresh surface for continuous reaction, and avoiding the risk of explosion of product gases.

5.2. Material Recycling

BOS slags mainly consist of CaO , SiO_2 , Fe_2O_3 , FeO , Al_2O_3 , MgO , MnO , and P_2O_5 , and their chemical component may vary with the furnace type, steel grades made, and pretreatment method. Recovery of metals (such as Fe, Mn, V, Cr and others) in metallurgical slags will not only increase the economic potential of slag but also solve the environmental problems induced by the harmful elements such as chromium (III) and vanadium (V) in the slags. Note the trivalent Cr (III) in the form of oxide is less toxic but it can be oxidized to harmful Cr (VI) at high oxygen concentrations or high MnO oxides. In general, the methods for recovering valuable metals/metal oxides from the BOS slags are categorized into physical separation,^[121–129] reduction process,^[130–136] and oxidation process.^[137–139]

5.2.1. Physical Separation

Physical separation methods, including magnetic separation and gravity separation, were reported to recover entrapped steel, vanadium, nickel, and chromium from BOS slags. For example, Anshan Iron and Steel Company recycles 0.28 million tons of grained steel with 60–65% Fe content and 0.4 million tons of iron concentrate with $\approx 50\%$ Fe content yearly from steelmaking slags through the combination of sorting, magnetic separation, and gravity concentration processes.^[122] A sorting–grinding–precise

reduction–magnetic separation process was developed by Gao et al.^[124] for waste steel reclamation, which enabled recovery of 29.8 kg iron particle and 152.1 kg iron-rich material from 1 ton of slag.

To enhance the separating efficiency between the target-element-enriched phases from BOS slag, the supergravity separation method was introduced to enrich the vanadium-containing spinel phase from vanadium slag produced in the BOS process^[125] and to separate the iron-bearing phase^[126] and phosphorus phase from BOS slag.^[127] In the processes, the molten slags were first heat treated properly to promote the target elements enriching in the target phases with large crystal size, and then supergravity technology was applied to separate the target phase from the molten slag. For example, a concentrate product with 25.19% V_2O_5 grade and 97.40% recovery ratio was obtained to enrich the vanadium-containing spinel phase from vanadium slag with the gravity coefficient $G = 900$, treat time $t = 20$ min, and temperature $T = 1557$ K.^[128]

Fe, Cr, Ni, and Mn could be directionally enriched in the spinel phase, as reported by Kim et al.,^[129] by controlling the primary crystalline and solidification process. The Cr and Mn contents increased up to 40% and 10%, respectively, in the controlled formation of a primary spinel phase. Metallic components in high-alloyed steelmaking slags were partially recovered using a physical separation process.

5.2.2. Reduction Process

This is based on the reduction of selected metal oxides at high temperatures using reducing agents such as C, Al, Si, FeSi, and SiC. In this process, valuable metals reduced from their oxides form an alloy with molten iron, and then can be recovered by separating the iron-bearing alloy from the slag. Recovering vanadium and chromium from BOS slag was reported using smelting reduction technique in a Tamman furnace, achieving the degree of metallization of slag 98% at 1600 °C for 30 min.^[130,131]

According to Qi et al.,^[132] the reduction ratios of iron and chromium in the stainless steel slag (SSS) improved on increasing the carbon equivalent added, reduction temperature, and basicity. The highest reduction ratio of Fe and Cr achieved was 93.92% and 72.76%, respectively, under the condition of carbon equivalent 2, reduction temperature 1600 °C, and binary basicity 1.2.^[133–135] Adamczyk et al.^[136] compared the efficiency of the reducing agents of C, Al, FeSi, and SiC for reduction of chromium in the SSS slag. Al was the strongest reducing agent; however, it leads to reducing a lot of SiO₂ because of the strong reactivity of aluminum. The reduction effect of FeSi was lower compared to C because releasing Si from FeSi consumed a large amount of energy, and also a part of Si and Fe sank to the bottom of the molten bath.^[136]

5.2.3. Oxidation Process

An alternative approach involving selective oxidation of typical transition metals (such as Fe, Mn, and V) in the metallurgical slags to magnetically susceptible compounds (such as Fe₃O₄ and Fe₂MnO₄) has been proposed by Semykina et al.^[137–139] This comprises controlled oxidizing of the transitional metals and subsequently separating magnetically susceptible compounds from the quenched slag by magnetic separation. This phase transformation favors magnetic separation of the target metal oxides from the waste slag in the late stage or the separation of the transformed phase (which is crystallized) from molten slag due to its low solubility in a given slag. This oxidation also occurred in the reaction of steam with molten BOS slag invented by Bhattacharjee et al.^[119] and Mukherjee and Bhattacharjee.^[120]

5.3. A Novel Process to Recover Energy and Materials from BOS Slag

Recently a novel process was developed by the present authors^[140–142] to recover thermal energy from molten BOS slag as syngas and hot gas, and recover valuable metals (Fe, Mn) in the form of magnetite by controlling the crystallization of the BOS slag after reacting the molten BOS slag with moisture. This process is based on the reaction of the molten steelmaking slag with the moist atmosphere (Figure 9). In addition to thermodynamic simulation, the process was experimentally verified by inline measuring H₂ production from the reaction of steam and molten BOS

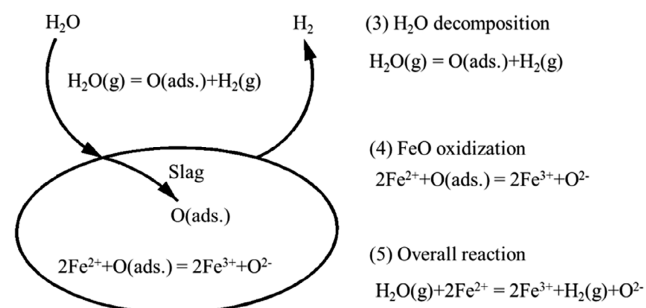


Figure 9. Schematic diagram of the reaction between molten CaO–SiO₂–FeO–MnO(–Al₂O₃–MgO) slag and moisture. Reproduced with permission.^[141] Copyright 2019, Springer Nature.

slags with different basicities and FeO concentrations. After reacting with steam, the BOS slag was subjected to controlled crystallization under the parameters selected (Figure 10), which promoted the nucleation and growth of magnetite, enabling its effective separation from slag by magnetic separation. The remaining slag can be used for construction materials or raw materials for the cement industry. This promising process provides a route to effectively recover both energy and materials from BOS slags and completely utilize the BOS slags. This novel process has been extensively studied in terms of the fundamental understanding of the reaction mechanisms, effects of processing parameters on hydrogen harvesting, and optimal conditions for controlled crystallization of targeted phases.^[140–142]

5.4. A Brief Summary on Energy and Material Recovery in BOS Slags

As summarized previously, recovery of energy and materials encompassed in BOS slags has attracted great attention. Dry (or wet) slag granulation has been extensively studied and implemented for blast furnace ironmaking slags to create glassy granules for the cement industry and for efficient heat recovery. However, this has not been applied to BOS slags due to the great difference in chemistry and the resultant high-temperature properties between blast furnace ironmaking slags and BOS slags. To recover the waste heat as chemical energy via endothermic reactions can be a useful route for the recovery of thermal heat in BOS slag. For the material recovery in BOS slag, various researches have been conducted to recover valuable metals such as Fe, Mn, Cr, and V in either metallic or oxides by physical separation, reduction process and oxidation process.

A novel process has recently been developed by the current authors to recover both waste heat (thermal and chemical energy) and valuable metals by reacting molten BOS slag with steam. The sensible heat and chemical energy in the BOS slag can be recovered in the form of syngas and hot gas, and the valuable materials can be recovered by magnetic separation after controlled crystallization and growth of magnetite. Finally the remaining slag can be used as raw materials in the cement industry or construction materials.

Overall, the recovery of energy and materials from high-temperature BOS slag is still a great challenge because of the lack of advanced technologies to achieve this, and this requires further research and development.

6. Conclusion

Since its commercialization in the 1950s, the BOS process has been rapidly established as a dominant process in global crude steel production. BOS slag, primarily a product of hot metal element (Si, Mn, Fe) oxidation and lime/dolomite dissolution, is of great importance to the production of high-quality crude steel at low costs as the old adage “Look after the slag and the metal will look after itself” is very appropriate. However, the behavior of BOS slag inside the BOS vessel (flux dissolution leading to slag formation and gas–slag–metal droplet reaction) is still not clear and its recycling has always been challenging. This article reviews the recent progress on the four important topics of BOS slags: 1) slag formation, i.e., dissolution of lime in the

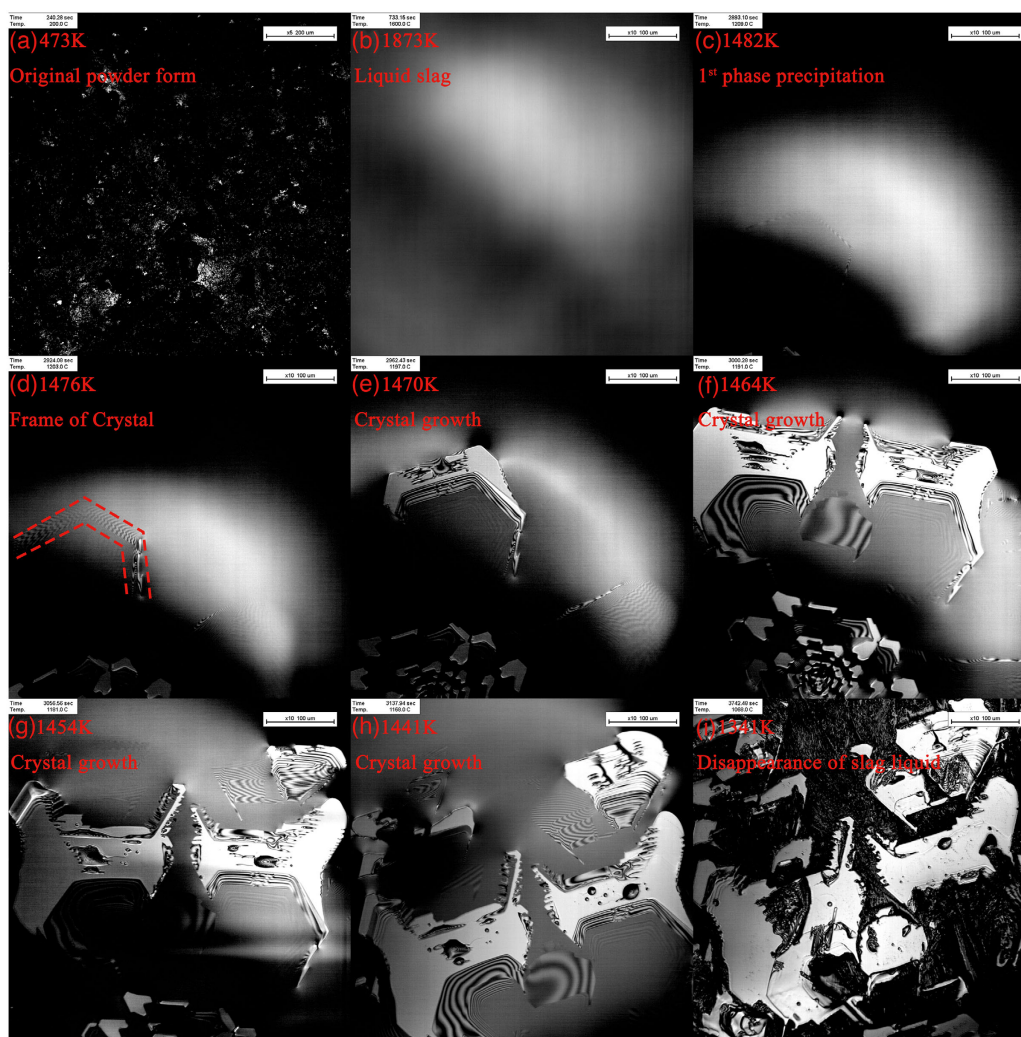


Figure 10. Direct observation of the crystallization process of a reacted slag at a continuous cooling rate of 10 K min^{-1} : a,b) morphology of mater slag (i.e., unreacted slag) at 473 and at 1873 K, respectively; c–i) crystallization process of the reacted slag at the temperature of 1482, 1476, 1470, 1464, 1454, 1359 K, respectively. Reproduced with permission.^[142] Copyright 2019, Springer Nature.

BOS slag; 2) high-temperature phase transformation of BOS slags; 3) transient phenomena in BOS slags due to metal droplet–slag–slag reactions; and 4) energy and material recovery from BOS slags. Continuous endeavor from the current authors to improve the fundamental understanding of BOS slags has also been included in this article. We intend in this article to provide the state-of-the-art understanding and point out the new research ideas in relevant research topics. This review is written based on a presentation given by the present authors in the 11th Molten Slags, Fluxes, Salts [MOLTEN2020] held virtually in February 21–25, 2021.^[143]

Acknowledgements

Z.L. would like to appreciate the financial support from Engineering and Physical Sciences Research Council (EPSRC) under the grant number EP/N011368/1 (EPSRC Fellowship). The authors are thankful for the financial support from EPSRC under the grant no. EP/M507829/1, from Innovate

UK under the project no. 102170, and from Tata Steel Europe. The authors would like to thank their respected colleagues and collaborators for their contributions to the reported researches.

Conflict of Interest

The authors declare no conflict of interest.

Keywords

basic oxygen steelmaking slag, energy recovery, gas–slag–metal reaction, high-temperature behavior, lime dissolution, material recovery, transient phenomena

Received: March 20, 2021
Revised: July 22, 2021
Published online: August 26, 2021

- [1] World Steel Association, Steel Statistical Yearbook 2019 (concise version), <https://www.worldsteel.org/en/dam/jcr:7aa2a95d-448d-4c56-b62b-b2457f067cd9/SSY19%2520concise%2520version.pdf> (accessed: March 2021).
- [2] T. Deng, J. Gran, D. Sichen, *Steel Res. Int.* **2010**, *81*, 347.
- [3] S. Amini, M. Brungs, O. Ostrovski, *ISIJ Int.* **2007**, *47*, 32.
- [4] B. Deo, K. Gupta, M. Malathi, P. Koopmans, A. Overbosch, R. Boom, in *The 5th European Oxygen Steelmaking Conf.*, Aachen, Germany, **2006**, p. 202.
- [5] E. Cheremisina, J. Schenk, L. Nocke, A. Paul, G. Wimmer, *ISIJ Int.* **2017**, *57*, 304.
- [6] M. Matsushima, S. Yadoomaru, K. Mori, Y. Kawai, *Trans. ISIJ* **1977**, *17*, 442.
- [7] S. H. Amini, M. P. Brungs, O. Ostrovski, S. Jahanshani, *Metall. Mater. Trans. B* **2006**, *37*, 773.
- [8] J. Pal, S. Ghorai, D. Singh, A. Upadhyay, S. Ghosh, D. Ghosh, D. Bandyopadhyay, *ISIJ Int.* **2010**, *50*, 105.
- [9] T. Deng, B. Glaser, D. Sichen, *Steel Res Int.* **2012**, *83*, 259.
- [10] T. Deng, D. Sichen, *Metall. Mater. Trans. B* **2012**, *43*, 578.
- [11] J. Martinsson, B. Glaser, D. Sichen, *Metall. Mater. Trans. B* **2018**, *49*, 3164.
- [12] L. M. Vieira, H. C. C. deOliveira, V. B. Telles, E. Junca, E. A. Vieira, J. R. de Oliveira, *J. Mater. Res. Technol.* **2020**, *9*, 14878.
- [13] N. Maruoka, A. Ishikawa, H. Shibata, S. Kitamura, *High Temp. Mater. Proc.* **2013**, *32*, 15.
- [14] S. Kitamura, *ISIJ Int.* **2017**, *57*, 1670.
- [15] Z. Li, M. Whitwood, S. Millman, J. van Boggelen, *Ironmaking Steelmak* **2014**, *41*, 112.
- [16] M. S. Millman, A. Kapilashrami, M. Bramming, D. Malmberg, Imphos: improving phosphorus refining, https://eur-lex.europa.eu/resource.html?uri=cellar:8a6cb7c-f77f-4ee7-bc38-9ebb13b52faf.0001.01/DOC_1&format=PDF (accessed: March 2021).
- [17] X. Guo, Z. Sun, J. Van Dyck, M. Guo, B. Blanpain, *Ind. Eng. Chem. Res.* **2014**, *53*, 6325.
- [18] L. Zhong, K. Mukai, M. Zeze, K. Miyamoto, N. Sano, *Steel Res Int.* **2007**, *78*, 236.
- [19] R. Sarkar, U. Roy, D. Ghosh, *Metall. Mater. Trans. B* **2016**, *47*, 2651.
- [20] N. Dogan, G. A. Brooks, M. A. Rhamdhani, *ISIJ Int.* **2009**, *49*, 1474.
- [21] N. Kikuchi, A. Matsui, Y. Uchida, *ISIJ Int.* **2020**, *60*, 922.
- [22] S. Manocha, F. Ponchon, *Metals* **2018**, *8*, 686.
- [23] B. Rout, G. Brooks, M. A. Rhamdhani, Z. Li, F. N. H. Schrama, J. Sun, *Metall. Mater. Trans. B* **2018**, *49*, 537.
- [24] W. Fix, H. Heymann, R. Heinke, *J. Am. Ceram. Soc.* **1969**, *52*, 346.
- [25] H. Suito, Y. Hayashida, Y. Takahashi, *Tetsu-to-Hagané* **1977**, *63*, 1252.
- [26] R. Inoue, H. Suito, *ISIJ Int.* **2006**, *46*, 174.
- [27] R. Inoue, H. Suito, *ISIJ Int.* **2006**, *46*, 188.
- [28] K. Shimauchi, S. Kitamura, H. Shibata, *Tetsu-to-Hagané* **2009**, *95*, 229.
- [29] M. Kami, M. Terasawa, A. Matsumoto, K. Ito, *Tetsu-to-Hagané* **2009**, *95*, 236.
- [30] Y. Kashiwaya, K. S. Pham, *Tetsu-to-Hagané* **2009**, *95*, 251.
- [31] R. Saito, H. Matsuura, K. Nakase, X. Yang, F. Tsukihashi, *Tetsu-to-Hagané* **2009**, *95*, 258.
- [32] S. Kitamura, K. Miyamoto, H. Shibata, N. Maruoka, M. Matsuo, *Tetsu-to-Hagané* **2009**, *95*, 313.
- [33] S. Khadhraoui, K. Hack, T. Jantzen, H. Odenthal, *Steel Res. Int.* **2019**, *90*, 1900085.
- [34] C. W. Bale, E. Bélisle, P. Chartrand, S. A. Decterov, G. Eriksson, A. E. Gheribi, K. Hack, I. H. Jung, Y. B. Kang, J. Melançon, A. D. Pelton, S. Petersen, C. Robelin, J. Sangster, P. Spencer, M. A. Van Ende, *Calphad* **2016**, *54*, 35.
- [35] Z. Li, W. Kockelmann, S. Zhang, *Presented at ICS2015 (6th International Congress on the Science and Technology of Steelmaking)*, Beijing, May 2015.
- [36] A. C. Hannon, *Nucl. Instr. Methods Phys. Res. Sect. A* **2005**, *551*, 88.
- [37] R. J. Hill, C. J. Howard, *J. Appl. Crystallogr.* **1987**, *467*.
- [38] *The Rietveld Method* (Ed.: R. A. Young), Oxford University Press, Oxford, UK **1993**.
- [39] N. Dogan, G. A. Brooks, *ISIJ Int.* **2011**, *51*, 1093.
- [40] B. Deo, A. Karamcheti, A. Paul, *ISIJ Int.* **1996**, *36*, 658.
- [41] M. S. Millman, A. Overbosch, A. Kapilashrami, D. Malmberg, M. Bramming, in *Proc. 3rd Int. Conf. on 'Process development in iron and steelmaking'*, Lulea, Sweden, June 2008.
- [42] Subagyo, G. A. Brooks, *ISIJ Int.* **2002**, *42*, 1182.
- [43] H. W. Meyer, W. E. Porter, G. C. Smith, J. Szekely, *J. Metals* **1968**, *35*.
- [44] A. Kadrolkar, N. Dogan, *Metall. Mater. Trans. B* **2019**, *50*, 2912.
- [45] S. Kitamura, H. Shibata, N. Maruoka, *High Temp. Mater. Process* **2012**, *31*, 195.
- [46] B. Rout, G. A. Brooks, M. K. Rhamdhani, Z. Li, F. N. H. Schrama, A. Overbosch, *Metall. Mater. Trans. B* **2018**, *49*, 1022.
- [47] N. Dogan, G. A. Brooks, M. A. Rhamdhani, *AISTech 2010 Proc.* **2010**, *1*, 1091.
- [48] T. Gare, G. S. F. Hazeldan, *Ironmaking Steelmaking* **1981**, *8*, 169.
- [49] R. J. Fruehan, L. J. Martonik, *Metall. Mater. Trans. B* **1974**, *5*, 1027.
- [50] T. Mohammed, S. Spooner, S. Sridhar, *JOM* **2014**, *66*, 1565.
- [51] M. S. Millman, A. Overbosch, A. Kapilashrami, D. Malmberg, M. Brämning, *Trans. Indian Inst. Met.* **2013**, *66*, 525.
- [52] S. Spooner, J. M. Warnett, R. Bhagat, M. A. Williams, S. Sridhar, *ISIJ Int.* **2016**, *56*, 2171.
- [53] C. Cicutti, M. Valdez, T. Pérez, R. Donayo, J. Petroni, *Lat. Am. Appl. Res.* **2002**, *32*, 237.
- [54] Subagyo, G. A. Brooks, K. S. Coley, *Can. Metall. Q* **2005**, *44*, 119.
- [55] G. A. Brooks, K. S. Coley, G. Irons, *ISIJ Int.* **2003**, *43*, 983.
- [56] S. Sabah, G. A. Brooks, *ISIJ Int.* **2014**, *54*, 836.
- [57] S. Sabah, G. A. Brooks, *Metall. Mater. Trans. B* **2014**, *46*, 863.
- [58] B. Rout, G. Brooks, Subagyo, M. A. Rhamdhani, Z. Li, *Metall. Mater. Trans. B* **2016**, *47*, 3350.
- [59] B. Rout, G. Brooks, M. A. Rhamdhani, Z. Li, F. N. H. Schrama, W. van der Knoop, *Metall. Mater. Trans. B* **2018**, *49*, 2191.
- [60] C. L. Molloseau, R. J. Fruehan, *Metall. Mater. Trans. B* **2002**, *33*, 335.
- [61] K. S. Coley, E. Chen, M. Pomeroy, in *Celebrating the Megascala: Proceedings of the Extractive and Processing Division* (Eds: P. J. Mackey, E. J. Grimsey, R. T. Jones, G. A. Brooks), TMS, **2014**, p. 289.
- [62] K. S. Coley, *J. Min. Metall. Sect. B Metall.* **2013**, *49*, 191.
- [63] E. Chen, K. S. Coley, *Ironmak. Steelmak.* **2010**, *37*, 541.
- [64] K. Coley, F. Ji, G. A. Brooks, M. A. Rhamdhani, Y. Pan, in *8th Int. Conf. on Molten Slags, Fluxes and Salts (MOLTEN 2009)*, (Eds: M. Sanchez, R. Parra, G. Riveros, C. Diaz), Santiago, Chile, **2009**, p. 727.
- [65] M. Lanyi, in *Flammability and Sensitivity of Materials in Oxygen-Enriched Atmospheres: Ninth Volume* (Eds: T. Steinberg, B. Newton, H. Beeson), ASTM International, West Conshohocken, PA **2000**, p. 163.
- [66] G. A. Brooks, M. A. Rhamdhani, K. S. Coley, Subagyo, Y. Pan, *Metall. Mater. Trans. B* **2009**, *40*, 353.
- [67] G. A. Brooks, Y. Pan, K. S. Coley, *Metall. Mater. Trans. B* **2005**, *36*, 525.
- [68] N. Dogan, G. A. Brooks, M. A. Rhamdhani, *ISIJ Int.* **2011**, *51*, 1086.
- [69] N. Dogan, G. A. Brooks, M. A. Rhamdhani, *ISIJ Int.* **2011**, *51*, 1102.
- [70] S. Spooner, Z. Li, S. Sridhar, *Metall. Mater. Trans. B* **2020**, *51*, 1301.
- [71] M. Ersson, A. Tilliander, L. Jonsson, P. Jönsson, *ISIJ Int.* **2008**, *48*, 377.
- [72] M. Ersson, L. Höglund, A. Tilliander, L. Jonsson, P. Jönsson, *ISIJ Int.* **2008**, *48*, 147.
- [73] N. Asahara, K. Naito, I. Kitagawa, M. Matsuo, M. Kumakura, M. Iwasaki, *Steel Res. Int.* **2011**, *82*, 587.
- [74] M. Ek, Q. F. Shu, J. van Boggelen, D. Sichen, *Ironmaking Steelmaking* **2012**, *39*, 77.
- [75] M. Swinnerton, Master Thesis, University of Wollongong, **2005**.

- [76] H. Suito, R. Inoue, *ISIJ Int.* **1995**, 35, 258.
- [77] S. Kitamura, S. Saito, K. Utagawa, H. Shibata, D. G. C. Robertson, *ISIJ Int.* **2009**, 49, 1838.
- [78] S. Basu, A. K. Lahiri, S. Seetharaman, J. Halder, *ISIJ Int.* **2007**, 47, 766.
- [79] M. S. Millman, A. Overbosch, A. Kapilashrami, D. Malmberg, M. Brämning, *Ironmaking Steelmaking* **2013**, 40, 460.
- [80] H. Gaye, P. V. Riboud, *Metall. Trans. B* **1977**, 8, 409.
- [81] P. V. Riboud, L. D. Lucas, *Can. Metall. Q.* **1981**, 20, 199.
- [82] M. A. Rhamdhani, G. A. Brooks, K. S. Coley, *Metall. Mater. Trans. B* **2006**, 37, 1087.
- [83] M. A. Rhamdhani, K. S. Coley, G. A. Brooks, *Metall. Mater. Trans. B* **2005**, 36, 591.
- [84] M. A. Rhamdhani, K. S. Coley, G. A. Brooks, *Metall. Mater. Trans. B* **2005**, 36, 219.
- [85] A. Jakobsson, M. Nasu, J. Mangwiru, K. C. Mills, S. Seetharaman, *Philos. Trans. R. Soc. A Math. Phys. Eng. Sci.* **1998**, 356, 995.
- [86] M. Wegener, L. Muhmood, S. Sun, A. V. Deev, *Ind. Eng. Chem. Res.* **2013**, 52, 16444.
- [87] J. Zhang, Q. Shu, S. Wei, *High Temp. Mater. Process.* **2003**, 22, 395.
- [88] K. Morohoshi, M. Uchikoshi, M. Isshiki, H. Fukuyama, *ISIJ Int.* **2013**, 53, 1315.
- [89] M. Nasu, K. C. Mills, B. J. Monaghan, A. Jakobsson, S. Seetharaman, *Ironmaking Steelmaking* **1999**, 26, 353.
- [90] A. Kasama, A. McLean, W. A. Miller, Z. Morita, M. J. Ward, *Can. Metall. Q.* **1983**, 22, 9.
- [91] K. Morohoshi, M. Uchikoshi, M. Isshiki, H. Fukuyama, *ISIJ Int.* **2011**, 51, 1580.
- [92] P. Sahoo, T. Debroy, M. J. McNallan, *Metall. Trans. B* **1988**, 19, 483.
- [93] S. Spooner, Z. Li, S. Sridhar, *Sci. Rep.* **2017**, 7, 5450.
- [94] A. N. Assis, J. Warnett, S. Spooner, R. J. Fruehan, M. A. Williams, S. Sridhar, *Metall. Mater. Trans. B* **2015**, 46, 568.
- [95] S. Spooner, A. N. Assis, J. Warnett, R. J. Fruehan, M. A. Williams, S. Sridhar, *Metall. Mater. Trans. B* **2016**, 47, 2123.
- [96] S. Spooner, A. N. Assis, J. Warnett, R. J. Fruehan, M. A. Williams, S. Sridhar, in *CTSSC-EMI Symp.*, Tokyo, Japan **2015**.
- [97] S. Spooner, A. Rahnama, J. M. Warnett, M. A. Williams, Z. Li, S. Sridhar, *Sci. Rep.* **2017**, 7, 14384.
- [98] M. Barati, E. Esfahani, T. A. Utigard, *Energy* **2011**, 36, 5440.
- [99] M. Sakakibara, *Tetsu-to-Hagane* **1990**, 76, 1587.
- [100] J. Ando, T. Nakahara, H. Onous, S. Ichimura, M. Kondo, *Techn. Rev.: Mitsubishi Heavy Industries* **1985**, 22, 136.
- [101] K. Yoshinaga, T. Fujii, T. Shigematsu, T. Nakata, *Tran ISIJ.* **1982**, 22, 823.
- [102] S. J. Pickering, N. Hay, T. F. Roylance, G. H. Thomas, *Ironmaking Steelmaking* **1985**, 12, 14.
- [103] D. Macauley, *Steel Times Int.* **1996**, 20, S15.
- [104] W. B. Featherstone, *Iron Steel Eng.* **1998**, 75, 42.
- [105] T. Mizuochi, T. Akiyama, T. Shimada, E. Kasai, J. Yagi, *ISIJ Int.* **2001**, 41, 1423.
- [106] S. Jahanshahi, D. Xie, Y. Pan, P. Ridgeway, J. Mathieson, in *1st Int. Conf. on Energy Efficiency and CO2 Reduction in the Steel Industry*, Dusseldorf, Germany, **2011**.
- [107] S. Ozawa, N. Sigaki, H. Tobo, *PRICM*, John Wiley & Sons, Inc., **2013**.
- [108] T. Akiyama, T. Shimada, E. Kasai, J. Yagi, in *China-Japan Int. Academic Symp.*, Sendai, Japan, **2000**.
- [109] E. Kasai, T. Kitajima, T. Akiyama, J. Yagi, F. Saito, *ISIJ Int.* **1997**, 37, 1031.
- [110] T. Shimada, T. Akiyama, E. Kasai, J. Yagi, *ISIJ Int.* **2000**, 40, 958.
- [111] T. Simada, V. Kochura, T. Akiyama, E. Kasai, J. Yagi, *ISIJ Int.* **2001**, 41, 111.
- [112] T. Mizuochi, T. Akiyama, T. Simada, E. Kasai, J. Yagi, *ISIJ Int.* **2001**, 41, 1423.
- [113] N. Maruoka, T. Mizuochi, H. Purwanto, T. Akiyama, *ISIJ Int.* **2004**, 44, 257.
- [114] N. Maruoka, K. Sato, J. Yagi, T. Akiyama, *ISIJ Int.* **2002**, 42, 215.
- [115] N. Maruoka, T. Akiyama, *ISIJ Int.* **2002**, 42, 1189.
- [116] Y. Qin, X. Lv, C. Bai, G. Qiu, P. Chen, *JOM*, **2012**, 64, 997.
- [117] Y. Qin, X. Lv, C. Bai, C. Pan, G. Qiu, *Steel Res. Int.*, **2013**, 84, 852.
- [118] Y. Qin, X. Lv, C. Bai, G. Qiu, in *Energy Technology 2012: Carbon Dioxide Management and Other Technologies*, (Eds: M. D. Salazar-Villalpando, N. R. Neelameggham, D. P. Guillen, S. Pati, G. K. Krumdick), John Wiley & Sons, Inc, Hoboken, NJ **2012**.
- [119] D. Bhattacharjee, T. Mukharjee, V. Tathavadkar, WO2007125537 A1, Tata Steel Limited, **2007**.
- [120] T. Mukherjee, D. Bhattacharjee, Tata Steel Limited), WO2007036953 A1, **2007**.
- [121] J. M. A. Geldenhuis, A. W. Home, in *85th Steelmaking Conf.* (Eds: D. L. Kanagy, D. J. Fuga, M. A. Baker), Iron and Steel Society of AIME, **2002**, p. 236.
- [122] H. Yi, G. Xu, H. Cheng, J. Wang, Y. Wan, H. Chen, *Proc. Environ. Sci.* **2012**, 16, 791.
- [123] K. Yu, Z. Zhou, B. Song, *Met. Mine Res. (in Chinese)*. **2010**, 1, 176.
- [124] J. Gao, S. Li, Y. Zhang, Y. Zhang, P. Chen, P. Shen, *Iron Steel Res Int.* **2011**, 18, 32.
- [125] J. Li, Z. Guo, J. Gao, *High Temp. Mater. Proc.* **2015**, 34, 61.
- [126] C. Li, J. Gao, Z. Guo, *Metall. Mat. Trans. B* **2016**, 47, 1516.
- [127] C. Li, J. Gao, Z. Wang, Z. Guo, *ISIJ Int.* **2017**, 57, 767.
- [128] J. Li, Z. Guo, J. Gao, *Ironmaking Steelmaking* **2014**, 41, 710.
- [129] E. Kim, J. Spooren, K. Broos, L. Horckmans, M. Quaghebeur, K. C. Vrancken, *Hydrometallurgy* **2015**, 158, 139.
- [130] B. Das, S. Prakash, P. S. R. Reddy, V. N. Misra, *Resour. Conserv. Recycl.* **2007**, 50, 4.
- [131] H. S. Park, B. C. Ban, K. S. Cho, *J. Korean Inst. Met. Mater.* **1994**, 32, 982.
- [132] Q. Qi, A. Xu, D. He, J. Pan, *Iron Steel.* **2017**, 52, 82.
- [133] F. Gu, Y. Zhang, Z. Su, Y. Tu, S. Liu, T. Jiang, *J. Cleaner Prod.* **2021**, 2, 126467.
- [134] K. Ohno, T. Miki, Y. Sasaki, M. Hino, *ISIJ Int.* **2008**, 48, 1368.
- [135] M. Leuchtenmüller, J. Antrekowitsch, S. Steinlechner, *Metall. Mater. Trans. B* **2019**, 50, 2221.
- [136] B. Adamczyk, R. Brenneis, C. Adam, D. Mudersbach, *Steel Res. Int.* **2010**, 81, 1078.
- [137] A. Semykina, J. Nakano, S. Sridhar, V. Shatokha, S. Seetharaman, *Metall. Mater. Trans. B.* **2010**, 41, 940.
- [138] A. Semykina, *Metall. Mater. Trans. B* **2012**, 43, 56.
- [139] A. Semykina, J. Nakano, S. Sridhar, V. Shatokha, S. Seetharaman, *Metall. Mater. Trans. B* **2011**, 42, 471.
- [140] J. Li, D. Bhattacharjee, X. Hu, D. Zhang, S. Sridhar, Z. Li, *Min. Process. Extract. Metall.* **2017**, 126, 94.
- [141] J. Li, D. Bhattacharjee, X. Hu, D. Zhang, S. Sridhar, Z. Li, *Metall. Mater. Trans. B* **2019**, 50, 1023.
- [142] J. Li, D. Bhattacharjee, X. Hu, D. Zhang, S. Sridhar, Z. Li, *Metall. Mater. Trans. B* **2019**, 50, 1931.
- [143] Z. Li, J. Li, S. Spooner, S. Seetharaman, BOS slag: formation, reaction, and energy and materials recovery (extended abstract), <http://wrap.warwick.ac.uk/149018> (accessed: February 2021).
- [144] W. Resch, PhD Thesis, Technical University, Clausthal, **1976**.
- [145] O. K. Tokovoi, A. I. Stroganov, D. Y. Povolotskii, *Steel USSR* **1972**, 116.
- [146] S. Koria, K. Lange, *Metall. Trans. B* **1984**, 15, 109.
- [147] I. Baptizmanskii, V. B. Okhotskii, K. S. Prosvirin, G. A. Shchedrin, Y. Ardelyan, *Steel USSR* **1977**, 7, 329.
- [148] H. W. Meyer, *J. Iron Steel Inst.* **1969**, 781.
- [149] R. F. Block, A. Masui, G. Stolzenberg, *Arch Eisenhüttenwes* **1973**, 44, 357.
- [150] R. C. Urquhart, W. G. Davenport, *Can. Metall. Quart.* **1973**, 12, 507.